

PCCP

Accepted Manuscript



This is an *Accepted Manuscript*, which has been through the Royal Society of Chemistry peer review process and has been accepted for publication.

Accepted Manuscripts are published online shortly after acceptance, before technical editing, formatting and proof reading. Using this free service, authors can make their results available to the community, in citable form, before we publish the edited article. We will replace this *Accepted Manuscript* with the edited and formatted *Advance Article* as soon as it is available.

You can find more information about *Accepted Manuscripts* in the [Information for Authors](#).

Please note that technical editing may introduce minor changes to the text and/or graphics, which may alter content. The journal's standard [Terms & Conditions](#) and the [Ethical guidelines](#) still apply. In no event shall the Royal Society of Chemistry be held responsible for any errors or omissions in this *Accepted Manuscript* or any consequences arising from the use of any information it contains.

Role of Lattice Defects in Catalytic Activities of Graphene Clusters for Fuel Cells

Lipeng Zhang^a, Quan Xu^c, Jianbing Niu^a, and Zhenhai Xia^{a,b,d,*}

^aDepartment of Materials Science and Engineering, North Texas, Denton, TX 76203, USA

^bDepartment of Chemistry, University of North Texas, Denton, TX 76203, USA

^cInstitute of New Energy, China University of Petroleum(Beijing) Beijing, China, 102248

^dSchool of Materials Science and Engineering, Northwestern Polytechnical University, Xi'an 710072, China

*Corresponding author: Email: Zhenhai.xia@unt.edu, Tel: 940-369-5805, Fax: 940-565-4824

Abstract

Defects are common but important in graphene, which could significantly tailor the electronic structures and physical and chemical properties. In this paper, the density functional theory (DFT) method was applied to study the electronic structure and catalytic properties of graphene cluster containing various point and line defects. The electron transfer processes in oxygen reduction reaction (ORR) on perfect and defective graphene cluster in fuel cells was simulated, and the free energy, reaction energy barrier of the elementary reactions were calculated to determine reaction pathways. It was found that the graphene cluster with point defect having pentagon rings at zigzag edge, or line defects (grain boundaries) consisting of pentagon-pentagon-octagon or pentagon-heptagon chains also at the edges, shows the electrocatalytic capability for ORR. Four-electron and two-electron transfer processes could occur simultaneously on graphene cluster with certain types of defects. The energy barriers of the reactions are comparable to that of platinum (111). The catalytic active sites were determined on the defective graphene.

Key words: graphene, DFT method, catalyst, defects, oxygen reduction reaction, fuel cells

Introduction

Graphene, a two dimensional monolayer structure of sp^2 hybridization carbon, has attracted great attention in a wide range of fields, such as electronics^{1,2}, sensors^{3,4}, batteries^{5,6} and catalysts⁷ owing to its exceptional physical and chemical properties⁸⁻¹⁰. It has been demonstrated that nitrogen-doped graphene can act as a metal-free electrode with three-time higher electrocatalytic activity, better long-term operation stability, and more tolerance to crossover effect than platinum for oxygen reduction reactions (ORR) in alkaline fuel cells⁷. With the potential of significantly reducing the cost of catalysts, graphene materials could eventually replace Pt in fuel cells, metal-air batteries and other energy conversion technologies, making them commercially viable. It is believed that the superior catalytic capabilities of the graphene materials are directly related to their nanostructure. A fundamental understanding of the structural effect on catalytic activities of this material will guide engineering the materials for more efficient catalysts, and even discovery of new catalysts.

Many factors, such as size, defects and doping, can tailor the structural, chemical and electrical properties of graphene materials. Among these factors, crystalline defects are the most common intrinsic structures existing in graphene materials. Several experimental studies have shown the occurrence of either native or physically introduced defects in graphene. Transmission electron microscopy (TEM)¹¹⁻¹⁵ and scanning tunneling microscopy (STM)^{16,17} have been used to directly observe the defects, including point defect (e.g., Stone-Wales defect, single vacancy^{12, 13, 16}, multiple vacancies^{18, 19}) and one dimensional defects or grain boundaries^{11, 20-22}. These point or line defects could change the local electronic structure or inject charge into the electron system of sp^2 -bonded carbon materials. Hou et al.²³ studied the electronic properties of graphene with native point defects and their effect to N doping on it. The formation energy, density of states of these defective graphene were calculated, and they concluded that the creation of defect before introducing N dopant would enhance the N doping of graphene. Density functional theory (DFT) is an effective theoretical method to study the electronic structures and catalytic activities and ORR pathways. The prominent pathways of ORR in proton exchange membrane (PEM)

fuel cells and the kinetics of the proposed non-electrochemical reactions were studied using DFT method²⁴, which is also applied in studying the mechanisms of ORR on carbon supported Fe-phthalocyanine (FePc/C), Co-phthalocyanine (CoPc/C) in alkaline solution²⁵, graphene, nitrogen doped graphene and cobalt-graphene-nitride systems²⁶⁻²⁸. Using the simulation methods, Ikeda, et al. explored nitrogen doped carbon based materials²⁹, and carbon alloy co-doped with boron and nitrogen materials³⁰ as catalysts of ORR in fuel cells. Recently, using DFT method, Zhang et al. studied the ORR mechanisms on nitrogen doped^{31, 32} and sulfur doped graphene^{33,34} in acidic environment. They proposed four electron transfer pathway on these doped graphene, and Stone-Wales defect could facilitate the ORR on the doped graphene. Wang et al.³⁵ proposed a possible way to enhance the ORR catalytic activity of N-doped graphene by controlling the degrees of hydrogenation of edges carbons with DFT method. Yu et al.³⁶ also explored the mechanisms of ORR on N-doped graphene in alkaline environment. Kaukonen et al.³⁷ used DFT method to explore the ORR on doped graphene, they found that single Ni, Pd, Pt, Sn, and P atoms embedded into divacancies in graphene were promising candidates for the cathode catalysts in fuel cells. However, little is known about the effect of the defects, especially for the intrinsic point and line defects on the capability of the graphene cluster for catalyzing ORR, a bottle neck in fuel cell performance.

In principle, ORR can process through direct four-electron transfer pathway, $O_2 + 4H^+ + 4e^- \rightarrow 2H_2O$, or two-electron transfer pathway in which hydrogen peroxide formed, $O_2 + 2H^+ + 2e^- \rightarrow H_2O_2$. The former pathway is expected to occur to achieve high efficiency. Thus, a route to search for an efficient catalyst is to determine if this catalyst facilitates the four-electron pathway. In this work, DFT method was used to study the ORR catalytic properties of the graphene cluster containing different types of point and line defects. The results show that some of these defective structures could facilitate the four-electron transfer in ORR, depending on the particular electronic structures modified by the defects and location of the defects.

Methods

Two types of graphene cluster models with defects were built based on experimental observations. One is the cluster containing zero dimensional defects, which include Stone-Wales defects (SW), vacancies with one (SV) or two (DV) carbon atom missing at the center³⁸, pentagon carbon rings substituting hexagon carbon rings at zigzag edge (PZ). The other is the cluster with grain boundaries, which are pentagons-heptagons connecting chains³⁹ or composed of octagons and fused pentagons^{40,41}. All graphene cluster edges are passivated by hydrogen atom. Unlike other point defects, a SW defect does not involve any removed or added atoms. Four hexagons are transformed into two pentagons and two heptagons (SW-5577) by rotating one of the C-C bonds by 90°, as shown in Figure 1 (b). Single vacancy (SV) by missing one carbon atom has been experimentally observed by TEM^{12,13} and STM¹⁶, as shown in Figure 1 (c). Double vacancies^{18,19} (DV) can be created either by the coalescence of two SVs or by removing two neighboring atoms; so two pentagons and one octagon appear instead of four hexagons in perfect graphene, as shown in Figure 1(d). In addition, when one atom is missing at zigzag or armchair edges of graphene, a pentagon is formed by reconstructing these edges. Figure 1(e) shows a pentagon ring at a zigzag edge. One-dimensional defects, also called line defects, can be thought of as a line of reconstructed point defects. The line defect is a line of alternative pairs of pentagons separated by octagons (GLD-558), as shown in Figure 1(f) and (g). The other 1D defect consists of alternative pentagons and heptagons (GLD-57), shown in Figure 1(h) and (i). There is odd number of octagon or heptagon rings on line defect for (f)-GLD-558-01 and (i)-GLD-57-01 but even number of octagon or heptagon rings on it for (g)-GLD-558-02 and (h)-GLD-57-02. These line defects have been observed in experiments^{11,20-22} and modeled by theoretical simulation methods^{3,42}.

The ORR process pathways over the perfect and defective graphene cluster as catalysts in acidic standard environment were simulated using the DFT. B3LYP hybrid density functional theory of Gaussian 09 (Revision A. 02; Gaussian, Inc; Wallingford, CT, 2009) was employed with a basis set of 6-31G (d, p)³², which can accurately describe the reaction process and explore the reaction mechanisms on carbon based nanomaterials, demonstrated by Alfred et al.²⁶⁻²⁸ and our previous work^{31,32}. In an acidic

environment, a unified mechanism for the first reduction step, which combines Damjanovic's proton participation in the first electron reduction step and Yeager's dissociative chemisorptions of O₂, is summarized as follows:



Or



where the asterisk represents a chemisorption site on graphene. In this step, we set OOH or O₂ near the graphene plane at a distance of 1.5~3.0 Å, and then observed if it was adsorbed at the possible catalytic active sites. After the first electron transfer, the succeeding electron transfer was simulated by continuously adding H atoms into the system. Because our simulation was applied in standard state, at 298K with the electropotential 0V and pH = 0, the reaction $\frac{1}{2} \text{H}_2 (1 \text{ atm}) \rightarrow \text{H}^+ + \text{e}^-$ is in equilibrium. For each step, we optimized the structures, and calculated the reaction free energy ΔG. Here, the free energy is defined as the difference between free energies of the initial and final states, which are calculated by the expression^{43,44}: $\Delta G = \Delta E + \Delta \text{ZPE} - T\Delta S + \Delta G_U$, where ΔE is reaction energy of reactant and product molecules adsorbed on catalyst surface, obtained from DFT calculations of optimization, ZPE is the zero point energy, S is the entropy, which are obtained from calculations of frequency, T is the temperature, and $\Delta G_U = -eU$, where U is the potential at the electrode, and e is the charge transferred. In addition, the reaction free energy in the aqueous solvation system was calculated, which was applied by adding key word SCRF⁴⁵ in Gaussian 09. This method places the graphene cluster reaction system in a cavity within the solvent reaction field. The Polarizable Continuum Model (PCM) using integral equation formalism variant (IEFPCM) was chosen as SCRF method⁴⁵. For the reaction with negative reaction free energy, it would occur spontaneously. The transition structure of each sub-reaction was searched using Synchronous Transit-Guided Quasi-Newton (STQN) method⁴⁶, which uses a linear synchronous transit

or quadratic synchronous transit approach to get closer to the quadratic region around the transition state and then uses a quasi-Newton or eigenvector-following algorithm to complete the optimization.

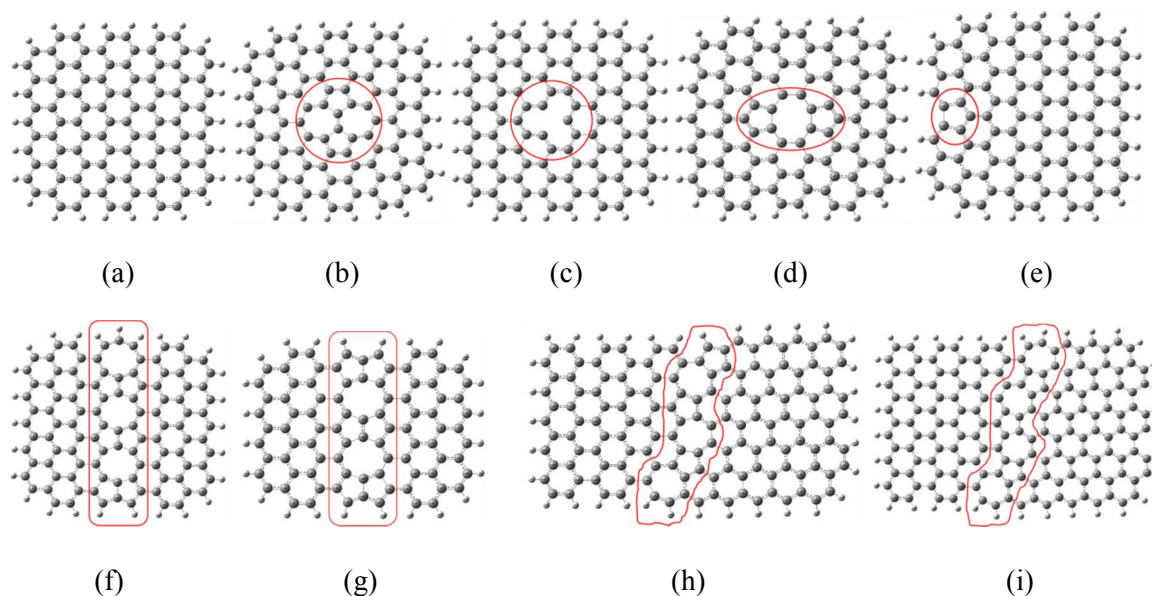


Figure 1. Perfect and defective graphene clusters. (a) Perfect graphene cluster, (b) Stone-Wales defect (SW), (c) Single vacancy (SV), (d) Double vacancies (DV), (e) Edge defect with pentagon ring at zigzag edge (PZ), Octagon and fused pentagon carbon rings line defect with (f) odd number of octagon rings (GLD-558-01) and (g) even number of octagon rings (GLD-558-02), and Pentagon-heptagon pairs line defects with (h) odd number of heptagon ring (GLD-57-01), and (i) even number of heptagon ring (GLD-57-02); The larger gray and smaller white balls denote to carbon and hydrogen atoms, respectively.

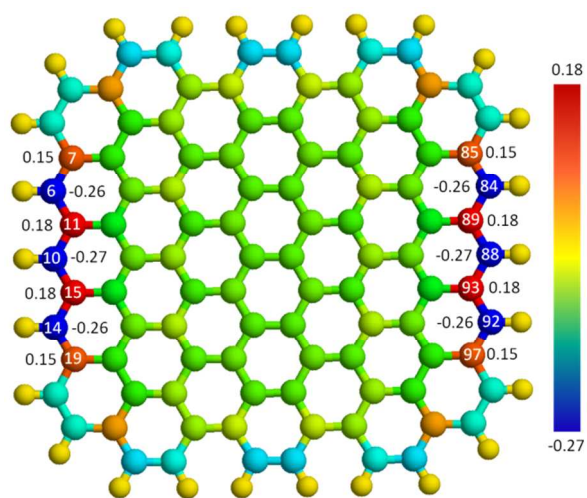
Results and Discussion

The electronic structure of the perfect and defective graphene clusters was determined and its effect on catalytic property was analyzed. Since those carbon atoms with high spin or charge density are most likely to be catalytic active sites^{31,32}, we have calculated spin and charge distributions on these defective graphenes, shown in Figure 2. There is no spin density on perfect graphene and defective ones with SW,

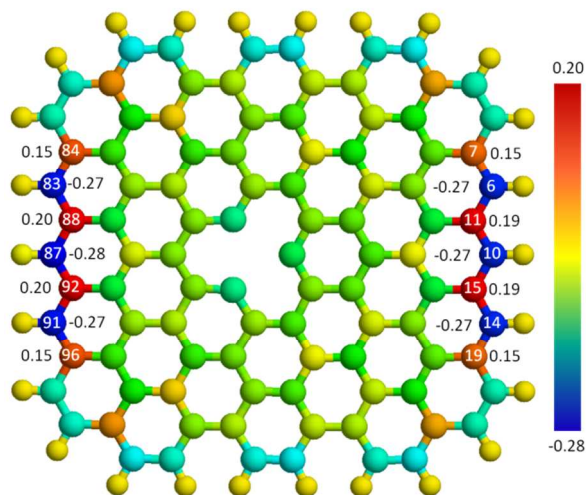
SV, and DV point defects or line defect structures GLD-558-02 and GLD-57-02 containing even number of octagon and heptagon carbon rings. The distribution of charge density on SW, SV and DV is similar with that on perfect graphene. Atoms with higher charge density distribute at zigzag edge, and the maximum value is less than 0.20, as shown in Figure 2 (a) and (b). Figure 2 (c) - (h) show the spin and charge densities of graphene cluster with pentagon ring at zigzag edge (PZ), line defects GLD-558-01 and GLD-57-01. For PZ, the high spin density appears at the zigzag edge opposite to the pentagon ring (e.g., C #87: 0.41, C #83: 0.27 in Figure 2c) while high charge density distributes at two zigzag edges. When the pentagon carbon ring locates at armchair edge or the center of graphene clusters, there is no spin density introduced into the graphene clusters. For GLD-558-01 structure, the atom possessing the highest spin density (0.41) locates in the octagon ring at the armchair edge. The high charge density distributions are more complex with a value of about 0.20, but mainly spread along zigzag edges, and octagon rings. For GLD-57-01 structure, the atom with higher spin density locates at zigzag edge (e.g. C#138: 0.44, C#139 and 140: 0.36) and the higher charge density distributes at zigzag sections of edge, their values are less than 0.22. For the SW defect, whatever the 5577 carbon ring locates, it does not introduce spin density on the graphene clusters. T. Yumura et al⁴⁷ found in their work that the existence of unpaired electrons in pristine hydrographenes depends on their edge shapes together with their size. The point defect–pentagon ring locating at zigzag edge and line defects–pentagon-pentagon-octagon chain and pentagon-heptagon chain change the edge shape of the defective graphene cluster, and induce local spin polarization, which mainly locate at the zigzag edge, some of them locate on the carbon atoms of defects themselves.

We studied the size effect of the graphene clusters on its electronic properties. The graphene clusters containing the same defects but with more carbon atoms (150 atoms for point defects, and 186 for line defects) were built and their spin and charge density distributions were calculated. Similar spin and charge distributions are found on the larger graphene clusters. Thus, the size effect of the defects is minimal on the electronic properties, especially spin and charge density distribution. This may be due to

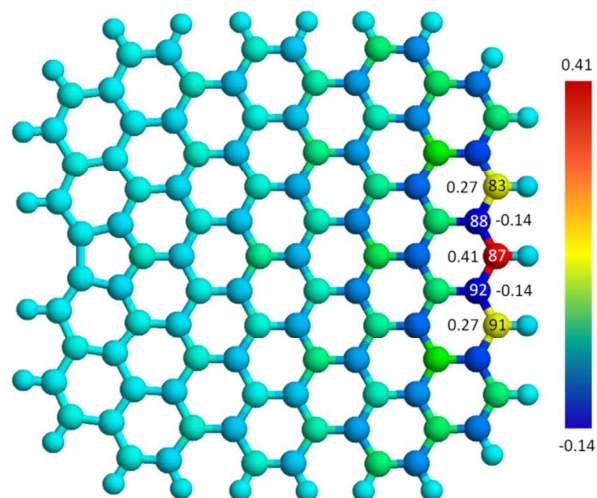
the fact that the disorder induced by these defects is very local and limited to a range within a nanometer, as observed in the experiment ⁴⁸.



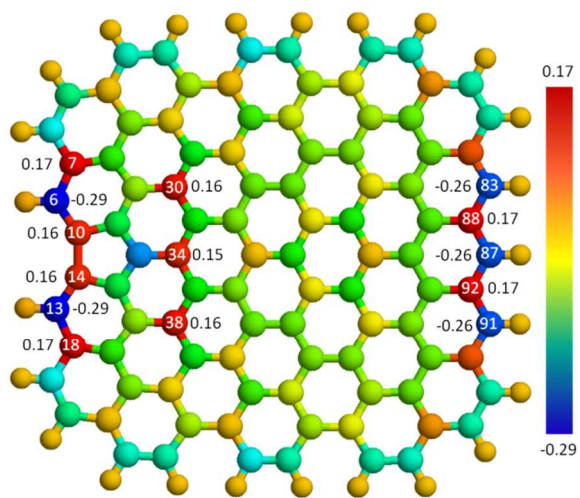
(a)



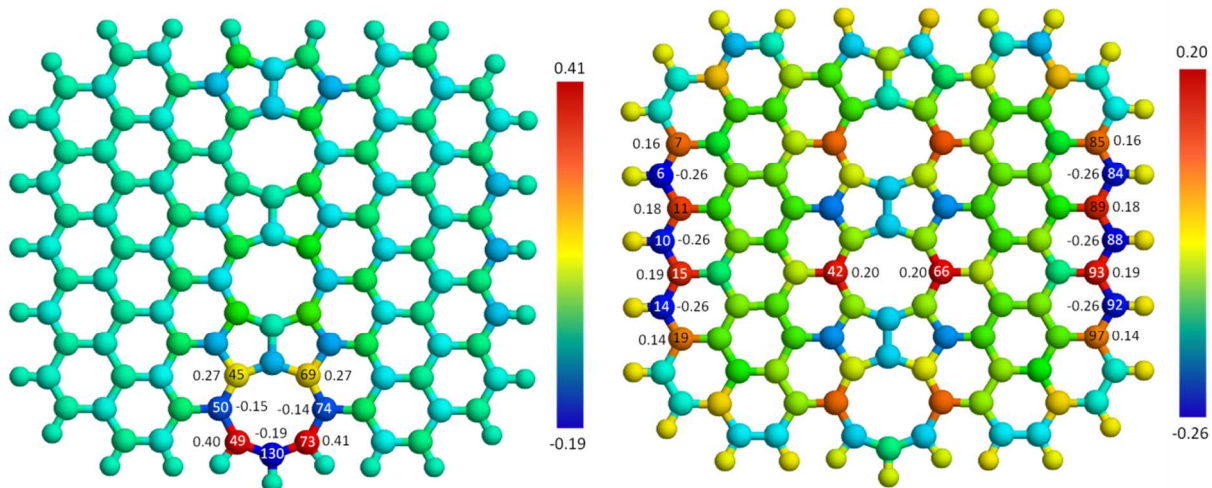
(b)



(c)

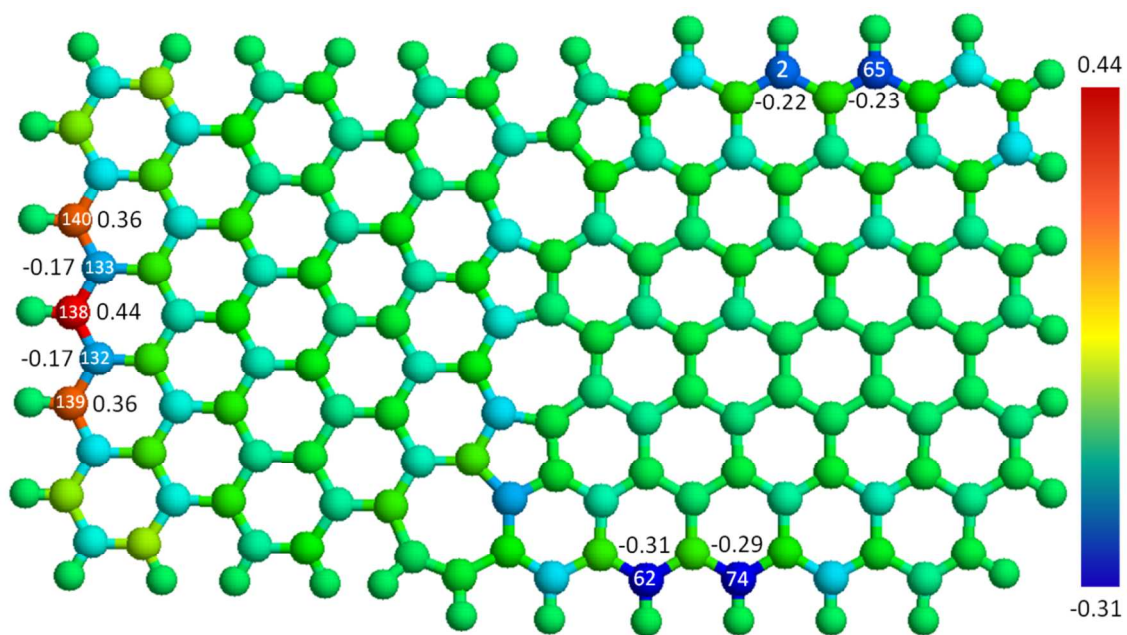


(d)



(e)

(f)



(g)

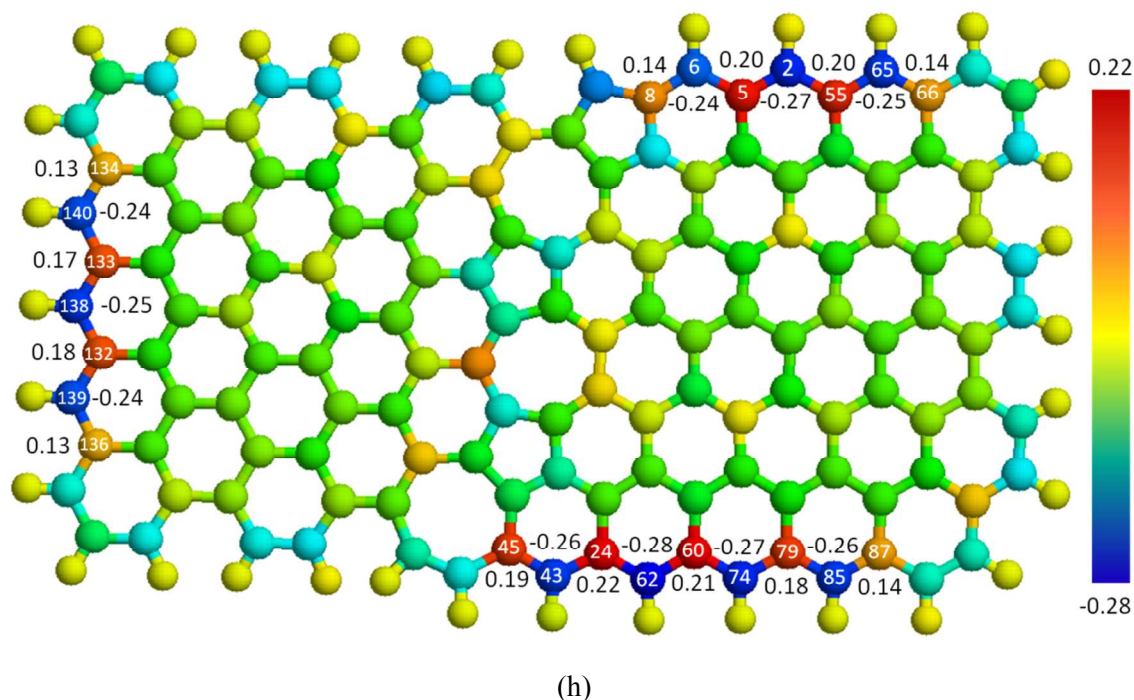


Figure 2. Charge and spin density distributions on perfect and defective graphene clusters: (a), (b), (d), (f) and (h) are charge density distribution on perfect, SV, PZ, GLD-558-01 and GLD-57-01 graphene clusters, respectively, while (c), (e) and (g) show spin density distribution on PZ, GLD-558-01 and GLD-57-01 graphene clusters, respectively. The color on the balls stands for different value, which is decrease in the color order red, orange, yellow, green, and blue.

OOH/O₂ adsorbing on the catalytic active sites is the first electron transfer in ORR, and a decisive step for a material to show catalytic capability. As mentioned above, in Damjanovic's proton participation mechanism in the first electron reduction step, oxygen molecule reacts with a proton to form OOH⁺. Following Damjanovic's proton participation and Yeager's dissociative chemisorptions of O₂, we simulate the first reaction step by checking if OOH/O₂ adsorbs on graphene surface or not. The catalytic capability of the defective graphene has been examined by introducing OOH or O₂ molecule over the atoms with high spin or charge density in a distance of 1.5 - 3.0 Å. For the perfect graphene and defective graphene structures with point defects, OOH or O₂ molecules cannot adsorb on these carbon atoms except for those with the pentagon ring. In the presence of a pentagon ring locating at zigzag edge as shown in Figure 3(a), OOH covalently bonds to the carbon atom #87 with the highest spin density, with a C-O

bond length of 1.45 Å. Therefore, among these point defects, only pentagon ring locating at zigzag edge structure shows the catalytic activities for ORR. For line defects, OOH/O₂ molecule can adsorb on the carbon atoms with spin density higher than 0.25 for GLD-588-01 and GLD-57-01 grain boundaries. These active sites are also located near the edge of the defective graphene, suggesting that the catalytic activities are the result of the synergistic effect between these defects and the corresponding edge structures. Here, the edge effect is critical to activate the catalytic activities of the defects on graphene. The range of the edge effect has been identified to be about 0.3 nm along the graphene edge, and the bonding structures are different from those inside the graphene⁴⁹. Therefore, with the edge effect, some type of defects can act as heteroatom dopants to promote ORR activities.

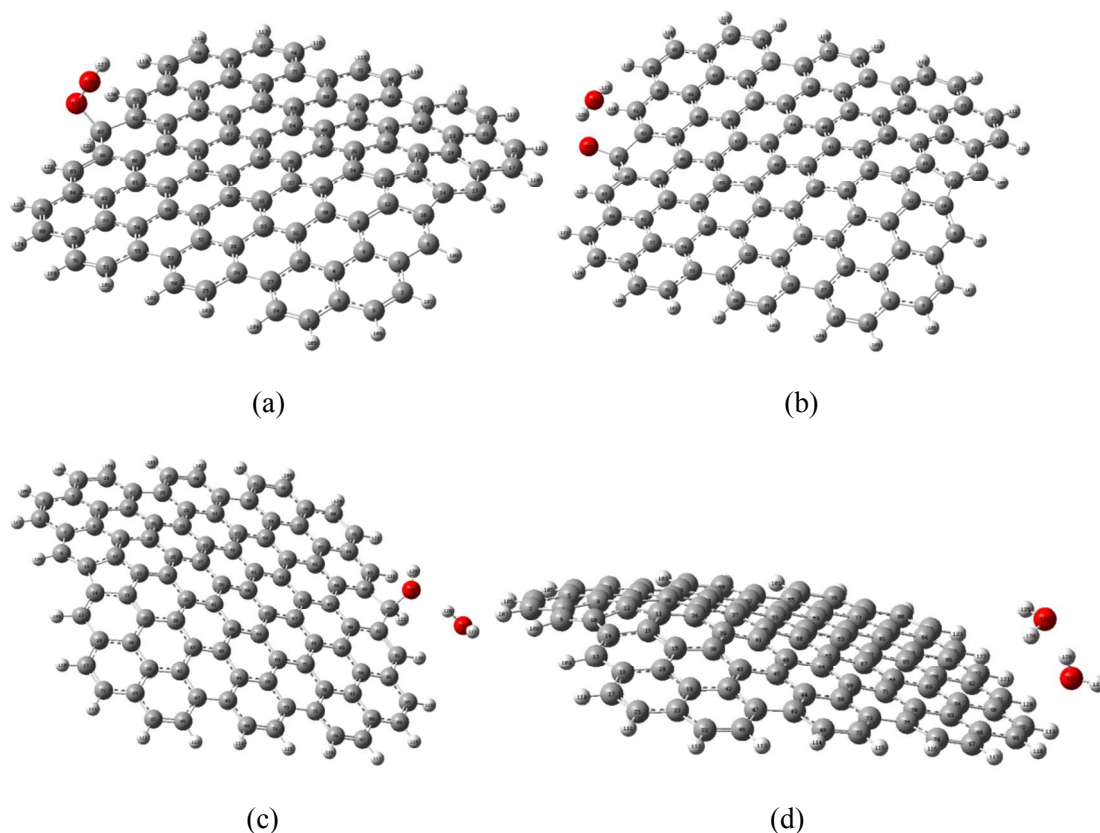
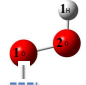
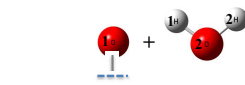
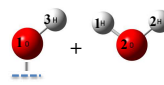
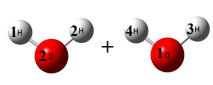


Figure 3. Four electron transfer processes of ORR on graphene with pentagon carbon ring at zigzag edge: (a) OOH adsorbed on carbon atom, (b) O-O bond breakage, and a water molecule formed, (c) OH molecule formed, and (d) two water molecules departing from graphene surface; The larger grey, red and smaller white balls denote to carbon, oxygen and hydrogen atoms, respectively.

Table 1. Distance variations (\AA) between characteristic atoms during ORR process

| |  |  |  |  | | |
|----------|---|---|--|---|-------|-------|
| | FS | TS | FS | FS | TS | FS |
| D(O1-G) | 1.446 | 1.435 | 1.352 | 1.463 | 1.686 | 3.473 |
| D(O1-O2) | 1.453 | 1.527 | 2.728 | 2.838 | 2.871 | 2.819 |
| D(O2-H1) | 0.973 | 0.973 | 0.971 | 0.965 | 0.975 | 0.964 |
| D(O2-H2) | | 1.703 | 0.966 | 0.976 | 0.965 | 0.978 |
| D(O1-H3) | | | | 0.969 | 0.974 | 0.967 |
| D(O1-H4) | | | | | 1.488 | 0.969 |

Note: D(O1-G) is the distance between the adsorbed oxygen atom in $^*\text{O}(1)\text{-OH}$ and graphene; D(O1-O2) is the distance between two different oxygen atoms in $^*\text{O}(1)\text{-O}(2)\text{H}$; D(O2-H1) is the distance between the non-adsorbed oxygen atom in $^*\text{O}-\text{O}(2)\text{H}$ and the first introduced H atom; D(O2-H2) is the distance between the non-adsorbed oxygen atom in $^*\text{O}-\text{O}(2)\text{H}$ and the second introduced H atom; D(O1-H3) is the distance between the adsorbed oxygen atom in $^*\text{O}(1)\text{-OH}$ and the third introduced atom; and D(O1-H4) is the distance between the adsorbed oxygen atom in $^*\text{O}(1)\text{-OH}$ and the fourth introduced atom. FS stands for final state of sub-reaction, TS stands for transition state of sub-reaction.

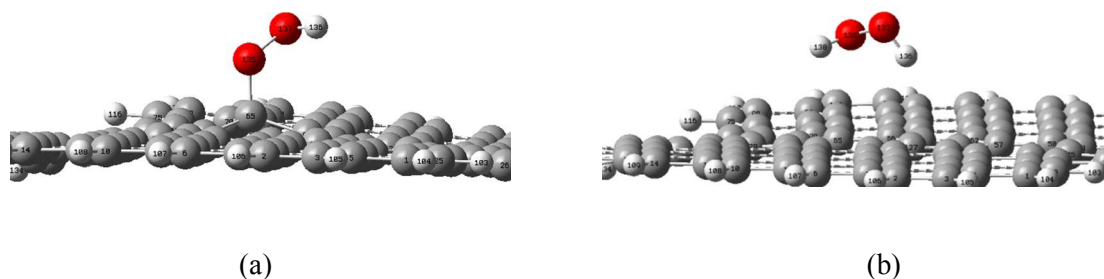


Figure 4. Two electron transfer processes of ORR on graphene with pentagon-pentagon-octagon chains (GLD-558-02) (because of the size reason, just show part of this structure): (a) OOH adsorbed on carbon atom #65, and (b) H_2O_2 molecule formed and departing from the graphene surface; The larger grey, red and smaller white balls denote to carbon, oxygen and hydrogen atoms, respectively.

After the first electron transfer, subsequent electron transfer reactions were determined by introducing protons into the system. When an H atom was introduced near the adsorbed OOH, it bonded to an oxygen atom, resulting in rupture of O-O bond and the formation of one water molecule while the other oxygen atom still adsorbs on the graphene, as shown in Figure 3(b). When the H atom bonded to the other oxygen

atom of OOH, two adsorbing OH were formed, which also led to the rupture of O-O bond. Since the reaction free energy (-0.93 eV) for forming O* and H₂O is lower than that of above reaction (-0.14 eV), the breakage of O-O prefers to form one adsorbed O and one water molecule. As mentioned above, the breakage of O-O bond is the key step of four-electron transfer, which defines the process being four-electron transfer pathway. When two more H atoms were sequentially introduced into the system, an OH first forms, followed by the generation of another water molecule, shown in Figure 3(c) and (d). These water molecules then depart from the graphene surface and the graphene recovers to its original state ready for another cycle of catalysis. Distance variations between these characteristic atoms (there is chemical bond formed or breakage) during ORR process described above are listed in Table 1, in which the transition states of O-O breakage and second water molecule departure from graphene cluster (see in Figure 6 (a)) sub-reactions are included. The overall ORR on GLD-558-01 and GLD-57-01 structures follows the similar process as described above. In addition to the four-electron transfer pathway, we also found the two-electron transfer reactions on GLD-558-02 and PZ structure. When the first electron transfer process finished, O₂ or OOH adsorbed on the carbon atoms (e.g., #61, and #65 on GLD-558-02; #94 on PZ), which possesses relatively low spin density (0.10~0.13). For the two-electron transfer reaction, when another H atom was introduced near the adsorbed OOH, it bonded to the oxygen atom bonding to the carbon atom on the graphene, forming a H₂O₂ molecule. The reaction processes on GLD-558-01 are shown in Figure 4 (a) and (b). Similar two-electron transfer processes were also found on PZ structure. So for these defective graphene showing catalytic activities, two-electron and four-electron transfer reactions take place simultaneously. Atoms locating at different position possess different spin or charge density because of defects, which make the bonding energy of O₂/OOH different, further affect the following sub-reaction. Some of these ORR are four-electron transfer reaction, while others follow two-electron transfer reaction pathway.

Although the defects that facilitate the four-electron transfer are observed in graphene, the electrocatalytic activities of defective graphene measured in the experiment are still much low compared

to hetero-element-doped graphene (e.g., N-doped graphene)⁷. The number of electron transfer for graphene is around 2.-2.5⁵⁰, indicating that two-electron transfer dominates the ORR on the undoped graphene. The lower catalytic activities of defective graphene may be attributed to the smaller number of active sites available on the graphene. As discussed above, in order to create active sites for catalyzing ORR, certain type of defects (e.g., pentagon) must locate within the range of edge effect. Generally speaking, the point defects distribute randomly within the graphene; the population of the point defects at the edge would be small. In the case of grain boundaries, the number of pentagons at the edge is also small although there are a large number of pentagons within the grain boundaries. Thus, the introduction of more edged defects could significantly improve the catalytic activities of the graphene cluster.

Table 2. Reaction free energy ΔG (eV) of four and two-electron transfer pathways of ORR on graphene clusters with point and line defects

| Reaction pathways | | Point defect (PZ) | | Line defect (GLD-558-01) | |
|------------------------|---|-------------------|---------------------|--------------------------|---------------------|
| | | In vacuum | In aqueous solution | In vacuum | In aqueous solution |
| Four electron transfer | $O_2 + H^+ + e^- \rightarrow *OOH$ | -1.20 | -1.22 | -1.29 | -1.60 |
| | $*OOH + H^+ + e^- \rightarrow *O + H_2O$ | -0.93 | -1.36 | -1.24 | -0.91 |
| | $*O + H^+ + e^- + H_2O \rightarrow *OH + H_2O$ | -2.01 | -1.78 | -1.35 | -1.21 |
| | $*OH + H^+ + e^- + H_2O \rightarrow 2H_2O$ | -0.62 | -0.57 | -1.09 | -1.19 |
| | Overall: $O_2 + 4H^+ + 4e^- \rightarrow 2H_2O$ | -4.76 | -4.93 | -4.97 | -4.91 |
| Two electron transfer | $O_2 + H^+ + e^- \rightarrow *OOH$ | -0.17 | -0.73 | -0.15 | -0.68 |
| | $*OOH + H^+ + e^- \rightarrow H_2O_2$ | -1.20 | -0.66 | -1.18 | -0.70 |
| | Overall: $O_2 + 2H^+ + 2e^- \rightarrow H_2O_2$ | -1.37 | -1.39 | -1.33 | -1.38 |

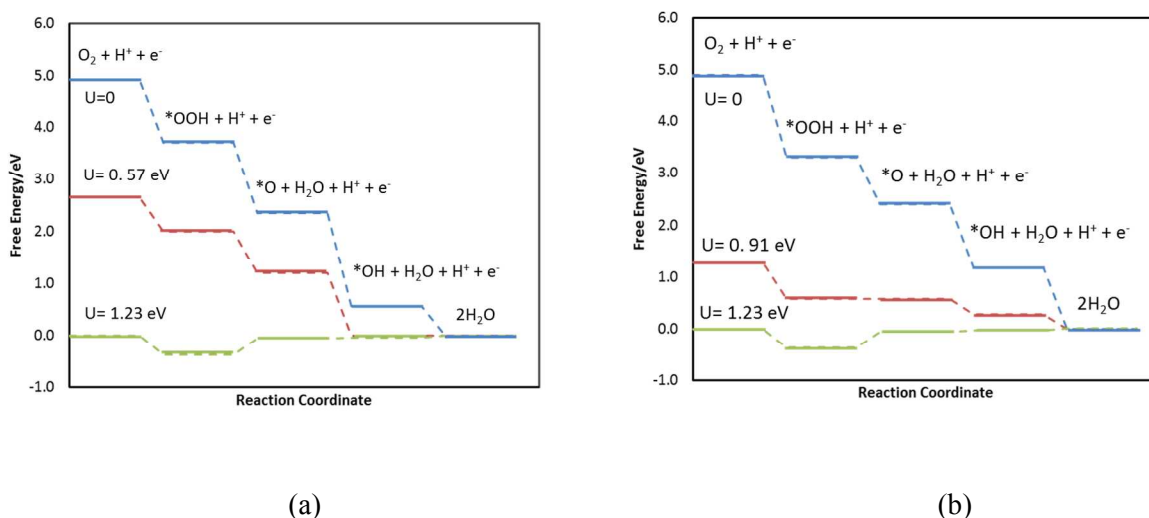


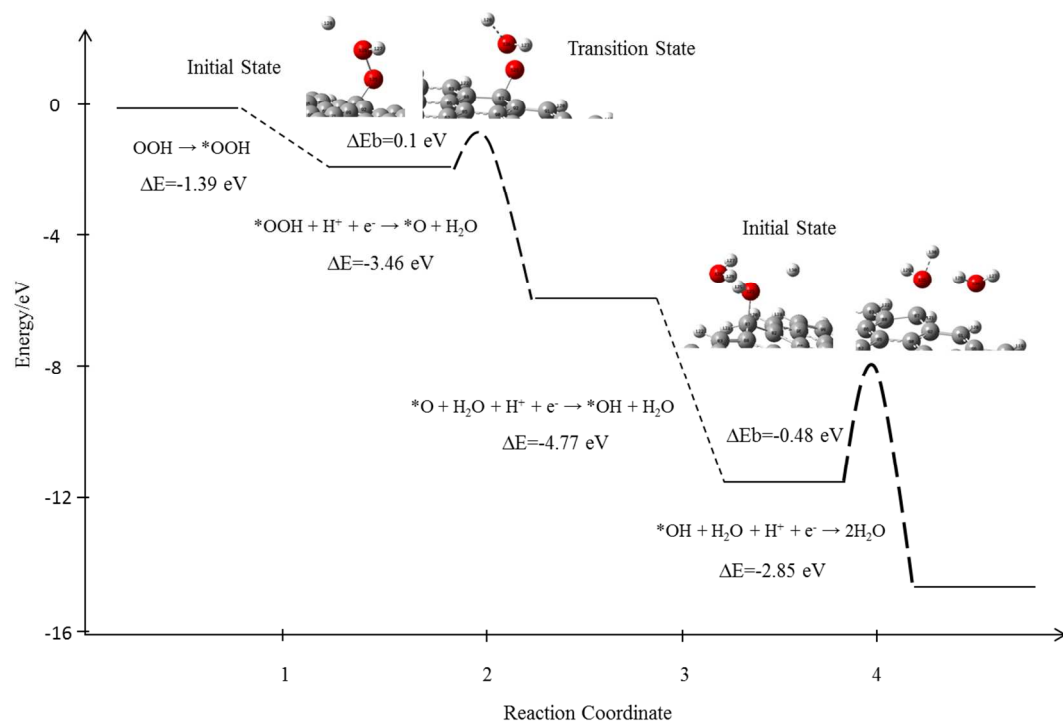
Figure 5. Reaction free energy diagram for four-electron transfer oxygen reduction reaction over graphene clusters with a pentagon carbon ring at zigzag edge (a) and a GLD-558-01 grain boundary (b) based on the energy of table 1. The blue lines show the results at zero cell potential ($U=0$), the red lines stand for the results at potential $U= 0.57\text{V}$ (a), and $U= 0.91\text{V}$ (b), and the green lines indicate the energy at potential $U= 1.23\text{ eV}$.

Reaction free energy ΔG of above electron transfer reaction processes were calculated for the graphene clusters with a pentagon carbon ring at zigzag edge and a GLD-558-01 grain boundary. Values of the free energy for electron transfer pathways in vacuum and aqueous environments are listed in Table 2. For the four electrons transfer ORR: $\text{O}_2 + 4\text{H}^+ + 4\text{e}^- \rightarrow 2\text{H}_2\text{O}$, the reaction free energy for the graphene cluster with pentagon carbon ring locating at zigzag edge and line defect GLD-558-01 in vacuum are -4.76 eV and -4.97 eV , respectively, whereas they are -4.93 eV and -4.91 eV in aqueous environments. So, the calculations including the solvent effect are closer to -4.92 eV standard reaction free energy of overall four-electron ORR⁴³. For two-electron transfer ORR: $\text{O}_2 + 2\text{H}^+ + 2\text{e}^- \rightarrow \text{H}_2\text{O}_2$, the reaction free energy for the two defective graphene clusters are -1.37 eV and -1.33 eV without considering the solvent effect, and -1.38 eV and -1.39 eV with solvent effect. Similarly, the results with the solvent effect are closer to experimental value -1.40 eV ²⁶. The solvent effects make the ΔG of the first sub-reaction more negative

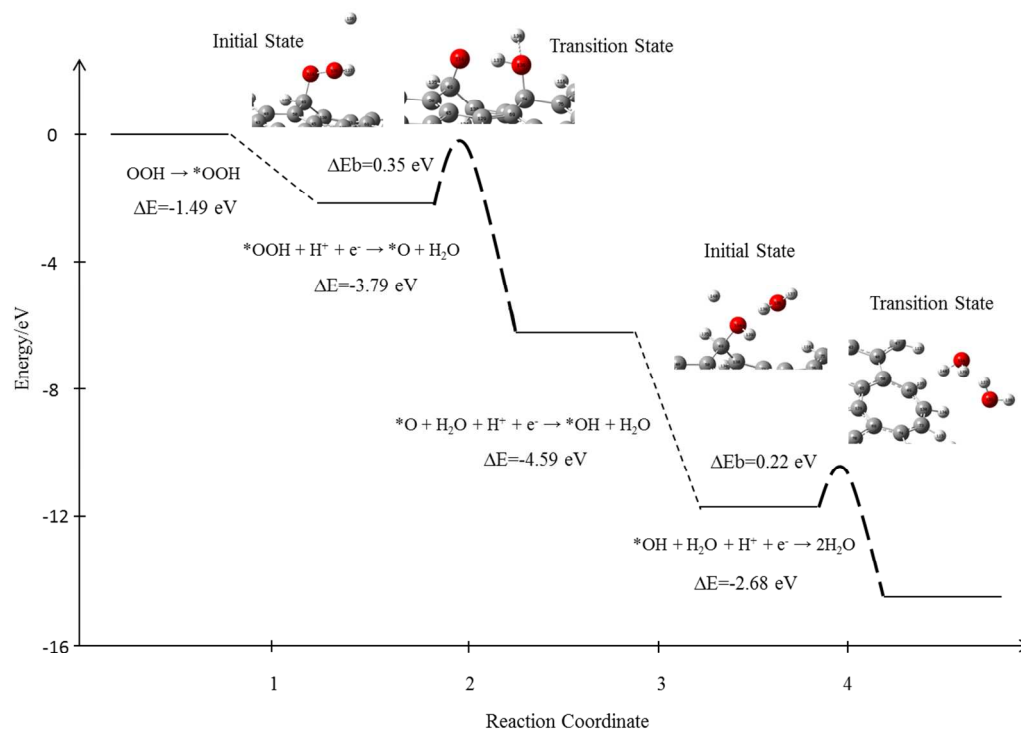
for both four-electron and two-electron transfer reaction, which means the solvent stabilized the adsorption of O₂ or OOH because of the formation of hydrogen bonds between them. This is consistent with the results obtained by Bao et al.³⁶. Thus, solvent effect must be considered in the calculation of free energy change for graphene catalysis. For each electron transfer reaction, ΔG is negative on both the defective graphene clusters, indicating that these sub-reactions could occur spontaneously in the view of thermodynamics. Compared to the point defect—pentagon carbon ring locating at zigzag edge, the values of ΔG for line-defect-GLD-558-01 are closer to the even value -1.23 eV. Relatively equal free energy in each reaction step may increase the reaction rate in ORR²⁶. Thus, the line-defect graphene would be more efficient in catalyzing the ORR. The free energy of four-electron transfer ORR over graphene clusters with pentagon ring at zigzag edge and GLD-558-01 at different potential are shown as Figure 5 (a) and (b). For the situation $U = 0$, all the sub-reaction steps are exothermic. If the potential $U = 1.23\text{V}$, the reaction of *OH departing is uphill, the reaction energy barriers is 0.66 V on graphene cluster with pentagon ring at zigzag edge. On graphene clusters with line-defect-GLD-558-01, the reaction of O-O rupture is uphill, the energy barrier is 0.30 V. The two energy barriers correspond to the experimentally observed overpotential. Thus, the reaction occurred on graphene clusters with line-defect-GLD-558-01 show the lower overpotential, which is favorable to the ORR catalytic activities. In this view, it also demonstrated that the graphene clusters with line-defect-558-01 could show the better catalytic properties.

The reaction free energy determines if ORR occurs thermodynamically. In order to explore the mechanisms of ORR further, energy barriers ΔE_b of each reaction was calculated, which determines the kinetics of the ORR catalytic activities. It is necessary to determine the transition states and reaction barriers of sub-reactions for four-electron transfer pathway on the cluster with point and line defects. Energy barriers ΔE_b is defined as the energy difference between the transition state and initial state during the sub-reaction. Here taking the reactions on PZ (shown in Figure 6(a)) and GLD-558-01 (shown in Figure 6(b)) as examples, the transition structure and reaction energy barriers were determined. For the first reaction step, we found that there is no reaction energy barrier for OOH molecule adsorbing on the

catalytic active sites of PZ and GLD-588-01 graphene clusters. The first step is not a limiting reaction step of the reaction kinetics, because the reaction energies of the first step are negative (-1.39 eV and -1.49 eV for PZ and GLD-588-01 graphene clusters, respectively) as shown in Figure 6. As mentioned above, the breakage of O-O bond is the key step of four-electron transfer pathway, the initial states, transition states (shown as inset of Figure 6 (a) and (b)) of this step are calculated for PZ and GLD-558-01 graphene clusters. In the case of PZ graphene cluster, OOH interacts with proton to form an adsorbed *O and a water molecule. The H was set near to the adsorbed OOH in different extension direction, and the structure with lowest energy was chosen as the initial state, in which the distance between introduced H atom to the adsorbing O atom is 2.7 Å. The transition state in this step is that OOH still adsorbs on the active site, but the introduced hydrogen is close to the OOH with a O-H distance of 1.9 Å. The energy barrier of this reaction is 0.1 eV. For GLD-558-01 graphene cluster, the products of the O-O bond breakage reaction are adsorbed *O and *OH on another carbon atom. This reaction experiences the transition state that the introduced hydrogen atom is close to the adsorbed *OH with the O-H distance of 1.55 Å. The reaction barrier is calculated to be 0.35 eV, which is higher than that on PZ graphene clusters. These energy barriers ΔE_b for the defective graphene clusters are comparable to those for platinum (111) surface⁵¹, nitrogen doped graphene, and nitrogen doped carbon nanotube⁵² (0.27 eV, 0.19 eV and 0.30 eV, respectively). There are no energy barriers found on PZ and GLD-558-01 graphene clusters in the third electron transfer step. However, in the last electron transfer step, the reaction barriers are 0.48 eV and 0.22 eV for PZ and GLD-558-01 graphene cluster, respectively. These values are also comparable to that ($\Delta E_b = 0.21$ eV) for the same reaction over platinum (111)⁵¹. Thus, pure graphene cluster could efficiently facilitate the ORR by introducing point defect like pentagon carbon ring at the edge, or line defect like pentagon-pentagon-octagon grain line. These defects interact with edge structure to generate active sites for ORR catalysis.



(a)



(b)

Figure 6. Reaction energy diagram of ORR on (a) PZ, and (b) GLD-558-01 defective graphene clusters

Conclusions

The effect of point- and line-defects in graphene cluster on the catalytic activities was studied using DFT methods. Among the point defects including Stone-Wale defect, single vacancy, double vacancies, and one substituting pentagon ring, only pentagon ring at zigzag edge has catalytic capability. In one dimensional line defects such as pentagon-heptagon chain (GLD-57) and pentagon-pentagon-octagon chain (GLD-558), the structure containing odd number of heptagon or octagon carbon ring generates spin density and can catalyze ORR. For those graphene clusters showing catalytic activity for ORR, the catalytic active sites usually locate at zigzag edge or at end of the pentagon-pentagon-octagon chains. Graphene edge plays an important role in activating the catalytic activities. The four-electrons and two-

electrons ORR can occur on these defective graphenes simultaneously, and these sub-reactions are energetically favorable since the reaction free energy of sub-reactions is negative. The reaction energy barriers of four-electron transfer pathway on defective graphene clusters are comparable to that of platinum.

Acknowledgements

The authors acknowledge the support from AFOSR MURI (FA9550-12-1-0037) and National Science Foundation (IIP- 1343270 and CMMI- 1363123).

References

- (1) Li, X. L.; Zhang, G. Y.; Bai, X. D.; Sun, X. M.; Wang, X. R.; Wang, E; Dai, H. J. *Nat. Nanotechnol.* **2008**, 3, 538–542.
- (2) Lee, C.; Wei, X.; Kysar, J. W.; Hone, J. *Science* **2008**, 321, 385–389.
- (3) Patil, A. J.; Vickery, J. L.; Scott, T. B.; Mann, S. *Adv. Mater.* **2009**, 21, 3159–3164.
- (4) Lu, C. H.; Yang, H. H.; Zhu, C. L.; Chen, X.; Chen, G. N. *Angew. Chem., Int. Ed.* **2009**, 48, 4785–4787.
- (5) Wu, Z. S.; Ren, W. C.; Xu, L.; Li, F.; Cheng, H. M. *ACS Nano* **2011**, 5, 5463–5471.
- (6) Yoo, E.; Kim, J.; Hosono, E.; Zhou, H.; Kudo, T.; Honma, I. *Nano Lett* **2008**, 8, 2277–2282.
- (7) Qu, L. T.; Liu, Y.; Baek, J. B.; Dai, L. M. *ACS Nano* **2010**, 4, 1321–1326.
- (8) Novoselov, K. S.; Jiang, Z.; Zhang, Y.; Morozov, S. V.; Stormer, H. L.; Zeitler, U.; Maan, J. C.; Boebinger, G. S.; Kim, P.; Geim, A. K. *Science* **2007**, 315, 1379.
- (9) Loh, K. P.; Bao, Q. L.; Ang, P. K.; Yang, J. X. *J. Mater. Chem.* **2010**, 20, 2277–2289.
- (10) Lee, C.; Wei, X. D.; Kysar, J. W.; Hone, J. *Science* **2008**, 321, 385–388.
- (11) Hashimoto, A.; Suenaga, K.; Gloter, A.; Urita, K.; Iijima, S. *Nature* **2004**, 430, 870–873.
- (12) Gass, M. H.; Bangert, U.; Bleloch, A. L.; Wang, P.; Nair, R. R.; Geim, A. K. *Nat. Nanotechnol.* **2008**, 3, 676–681.
- (13) Meyer, J. C.; Kisielowski, C.; Erni, R.; Rossell, M. D.; Crommie, M. F.; Zettl, A. *Nano Lett.* **2008**, 8, 3582–3586.

- (14) Warner, J. H.; Rummeli, M. H.; Ge, L.; Gemming, T.; Montanari, B.; Harrison, N. M.; Büchner, B.; Briggs, G. A. D. *Nat. Nanotechnol.* **2009**, *4*, 500–504.
- (15) Girit, C. O.; Meyer, J. C.; Erni, R.; Rossell, M. D.; Kisielowski, C.; Yang, L.; Park, C.-H.; Crommie, M. F.; Cohen, M. L.; Louie, S. G. *Science* **2009**, *323*, 1705–1708.
- (16) Ugeda, M. M.; Brihuega, I.; Guinea, F.; Gómez-Rodríguez, J. M. *Phys. Rev. Lett.* **2010**, *104*, 096804.
- (17) Tapasztó, L.; Dobrik, G.; Nemes-Incze, P.; Vertesy, G.; Lambin, P.; Biró, L. P. *Phys. Rev. B* **2008**, *78*, 233407.
- (18) Krasheninnikov, A. V.; Lehtinen, P. O.; Foster, A. S.; Nieminen, R. M. *Chem. Phys. Lett.* **2006**, *418*, 132–136.
- (19) El-Barbary, A. A.; Telling, R. H.; Ewels, C. P.; Heggie, M. I.; Briddon, P. R. *Phys. Rev. B* **2003**, *68*, 144107.
- (20) Coraux, J.; N'Diaye, A. T.; Busse, C.; Michely, T. *Nano Lett.* **2008**, *8*, 565–570.
- (21) Červenka, J.; Katsnelson, M. I.; Flipse, C. F. J. *Nat. Phys.* **2009**, *5*, 840–844.
- (22) Lahiri, J.; Lin, Y.; Bozkurt, P.; Oleynik, I. I.; Batzill, M. *Nat. Nanotechnol.* **2010**, *5*, 326–329.
- (23) Hou Z.; Wang X.; Ikeda, T.; Terakura, K.; Oshima, M.; Kakimoto, M.; Miyata, S.; *Phys. Review B* **2012**, *85*, 165439.
- (24) Stephen, W.; Abhishek, D.; Masoud, A.; Heinz, P. *J. Phys. Chem. C* **2008**, *112*, 8464–8475.
- (25) Chen, R. R.; Li, H. X.; Chu, D.; Wang, G. F. *J. Phys. Chem. C* **2009**, *113*, 20689–20697.
- (26) Reyimjan, A.; Sidik; Alfred, B. A. *J. Phys. Chem. B* **2006**, *110*, 1787–1793.
- (27) Ellen, V.; Alfred, B. A. *J. Phys. Chem. C* **2007**, *111*, 9330–9336.
- (28) Kiera, A.; Kurak; Alfred, B. A. *J. Phys. Chem. C* **2009**, *113*, 6730–6734.
- (29) Ikeda, T.; Boero, M.; Huang, S.; Terakura, K.; Oshima, M.; Ozaki, J.; Miyata, S.; *J. Phys. Chem. C* **2010**, *114* (19), 8933-8937.
- (30) Ikeda, T.; Boero, M.; Huang, S. Terakura, K.; Oshima, M.; and Ozaki, J.; *J. Phys. Chem. C* **2008**, *112*, 14706-14709
- (31) Zhang, L.; Xia, Z. *J. Phys. Chem. C* **2011**, *115*, 11170-11176.
- (32) Zhang, L.; Niu, J.; Dai, L.; Xia, Z. *Langmuir* **2012**, *28*, 7542-7550.
- (33) Jeon, I.; Zhang, S.; Zhang, L. Choi, H.; Xia, Z.; Dai, L.; Baek, J. *Adv. Mater.* **2013**, *25*, 6138-6145.

- (34) Zhang, L.; Niu, J.; Li, M.; Xia, Z. *J. Phys. Chem. C* **2014**, 118, 3545-3553.
- (35) Wang, X.; Hou, Z.; Ikeda, T.; Huang, S.; Terakura, K.; Boero, M.; Oshima, M.; Kakimoto, M. Miyata, S.; *Phys. Review B* **2011**, 84, 245434.
- (36) Yu, L.; Pan, X.; Cao, X.; Hu, P.; Bao, X. *J. Catal.* **2011**, 282, 183-190.
- (37) Kaukonen, M.; Krasheninnikov, A. V. ; Kauppinen, E.; Nieminen, R. M.; *ACS Catal.* **2013**, 3 (2), 159-165.
- (38) Banhart, F.; Kotakoski, J.; Krasheninnikov, A. V. *ACS Nano* **2011**, Vol.5, 26-41.
- (39) Huang, P. Y., Ruiz-Vargas, C. S.; Zande, A. M.; Whitney, W. S.; Levendorf, M. P.; Kevek, J. W.; Garg, S.; Alden, J. S.; Hustedt, C. J.; Zhu, Y.; Park, J.; Mc Euen, P. L.; Muller, D. A. *Nature*, **2011**, Vol. 469, 389-393.
- (40) Gunlycke, D.; White, C. T. *PRL* **2011**, 106, 136806
- (41) Hashimoto, A.; Suenaga, K.; Gloter, A.; Urita, K.; Iijima, S. *Nature* **2004**, 430, 870-873.
- (42) Lin, X.; Ni, J. *Phys. Rev. B* **2011**, 84, 075461
- (43) Nørskov, J. K. ; Rossmeisl, J.; Logadottir, A.; Lindqvist, L. *J. Phys. Chem. B* **2004**, 108, 17886-17892.
- (44) Joseph W. Ochtershi; *Thermochemistry in Gaussian*, **2000**, Gaussian, Inc.
- (45) Cossi, M.; Rega, N.; Scalmani, G.; and Barone, V.; *J. Comp. Chem.*, **2003**, 24 669-681
- (46) Peng, C.; Schlegel, H. B.; *Israel J. of Chem.*, **1993**, 33, 449.
- (47) Yumura, T.; Kobayashi, H.; Yamabe, T.; *The J. Chem. Phys.* **2010**, 133, 174703.
- (48) Rutter, G. M.; Grain, J. N.; Guisinger, N. P.; Li, T.; First, P. N.; Stroschio, J. A.; *Science* **2007**, 317, 219-222.
- (49) Li, M.; Zhang, L.; Xu, Q.; Niu, J.; Xia, Z. *Journal of Catalysis* **2014**, 314, 66-72.
- (50) Wang, S.; Yu, D.; Dai, L.; Chang, D.; Baek, J. *ACS NANO* **2011**, 5, 6202-6209
- (51) Sha, Y.; Yu, T.; Liu, Y.; Merinov, B.; Goddard III, W. *J. Phys. Chem. Lett.* **2010**, 1 856-861.
- (52) Ni, S.; Li, Z.; Yang, J. *Nanoscale* **2012**, 4, 1184-1189.

Tables

Table 1. Distance variations (Å) between characteristic atoms during ORR process

| | FS | TS | FS | TS | TS | FS | |
|----------|-------|-------|-------|-------|-------|-------|--|
| D(O1-G) | 1.446 | 1.435 | 1.352 | 1.463 | 1.686 | 3.473 | |
| D(O1-O2) | 1.453 | 1.527 | 2.728 | 2.838 | 2.871 | 2.819 | |
| D(O2-H1) | 0.973 | 0.973 | 0.971 | 0.965 | 0.975 | 0.964 | |
| D(O2-H2) | | 1.703 | 0.966 | 0.976 | 0.965 | 0.978 | |
| D(O1-H3) | | | | 0.969 | 0.974 | 0.967 | |
| D(O1-H4) | | | | | 1.488 | 0.969 | |

Note: D(O1-G) is the distance between the adsorbed oxygen atom in *O(1)-OH and graphene; D(O1-O2) is the distance between two different oxygen atoms in *O(1)-O(2)H; D(O2-H1) is the distance between the non-adsorbed oxygen atom in *O-O(2)H and the first introduced H atom; D(O2-H2) is the distance between the non-adsorbed oxygen atom in *O-O(2)H and the second introduced H atom; D(O1-H3) is the distance between the adsorbed oxygen atom in *O(1)-OH and the third introduced atom; and D(O1-H4) is the distance between the adsorbed oxygen atom in *O(1)-OH and the fourth introduced atom. FS stands for final state of sub-reaction, TS stands for transition state of sub-reaction

Table 2. Reaction free energy ΔG (eV) of four and two-electron transfer pathways of ORR on graphene clusters with point and line defects

| Reaction pathways | | Point defect (PZ) | | Line defect (GLD-558-01) | |
|------------------------|---|-------------------|---------------------|--------------------------|---------------------|
| | | In vacuum | In aqueous solution | In vacuum | In aqueous solution |
| Four electron transfer | $O_2 + H^+ + e^- \rightarrow *OOH$ | -1.20 | -1.22 | -1.29 | -1.60 |
| | $*OOH + H^+ + e^- \rightarrow *O + H_2O$ | -0.93 | -1.36 | -1.24 | -0.91 |
| | $*O + H^+ + e^- + H_2O \rightarrow *OH + H_2O$ | -2.01 | -1.78 | -1.35 | -1.21 |
| | $*OH + H^+ + e^- + H_2O \rightarrow 2H_2O$ | -0.62 | -0.57 | -1.09 | -1.19 |
| | Overall: $O_2 + 4H^+ + 4e^- \rightarrow 2H_2O$ | -4.76 | -4.93 | -4.97 | -4.91 |
| Two electron transfer | $O_2 + H^+ + e^- \rightarrow *OOH$ | -0.17 | -0.73 | -0.15 | -0.68 |
| | $*OOH + H^+ + e^- \rightarrow H_2O_2$ | -1.20 | -0.66 | -1.18 | -0.70 |
| | Overall: $O_2 + 2H^+ + 2e^- \rightarrow H_2O_2$ | -1.37 | -1.39 | -1.33 | -1.38 |

Figure Captions

Figure 1. Perfect and defective graphene clusters. (a) Perfect graphene, (b) Stone-Wales defect (SW), (c) Single vacancy (SV), (d) Double vacancies (DV), (e) Edge defect with pentagon ring at zigzag edge (PZ), Octagon and fused pentagon carbon rings line defect with (f) odd number of octagon rings (GLD-558-01) and (g) even number of octagon rings (GLD-558-02), and Pentagon-heptagon pairs line defects with (h) odd number of heptagon ring (GLD-57-01), and (i) even number of heptagon ring (GLD-57-02); The larger gray and smaller white balls denote to carbon and hydrogen atoms, respectively.

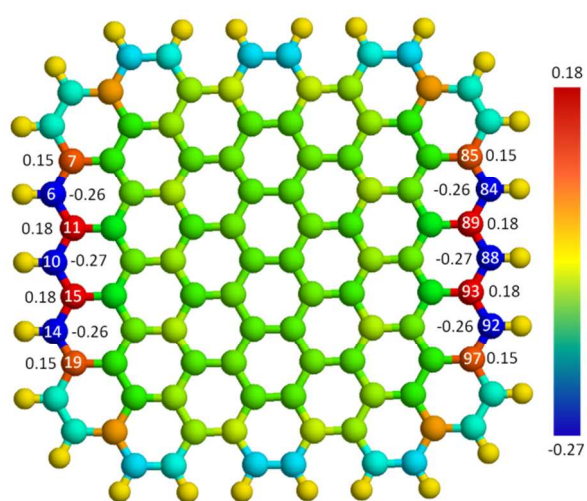
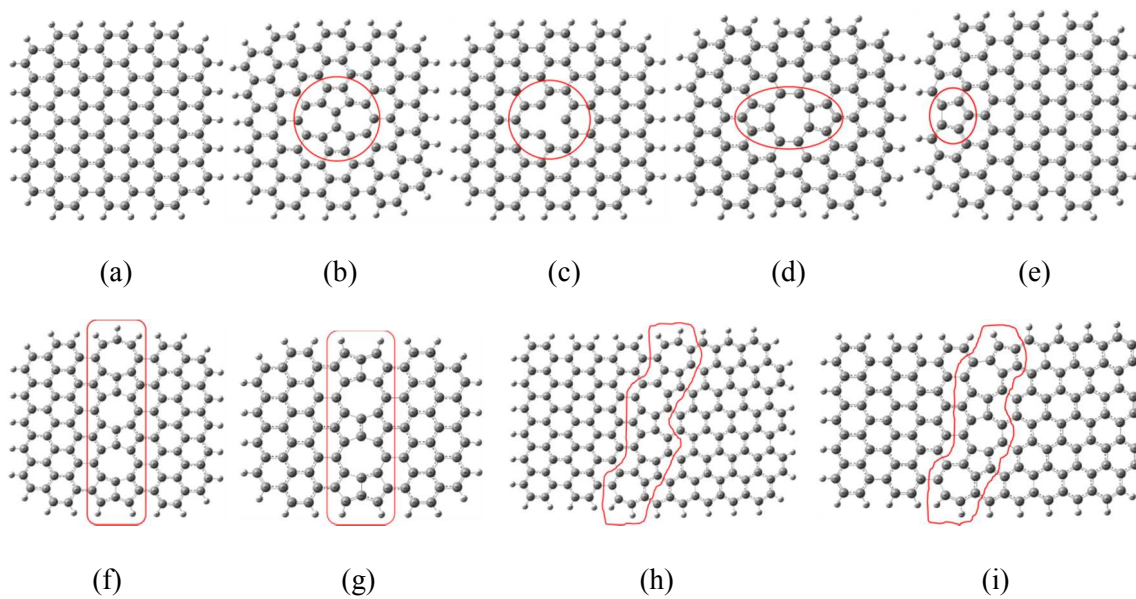
Figure 2. Charge and spin density distribution on perfect and defective graphene clusters: (a), (b), (d), (f) and (h) are charge density distribution on perfect, SV, PZ, GLD-558-01 and GLD-57-01 graphene clusters, respectively, while (c), (e) and (g) show spin density distribution on PZ, GLD-558-01 and GLD-57-01 graphene clusters, respectively. The color on the circle stands for different value, which is decrease in the color order red, orange, yellow, green, and blue.

Figure 3. Four electron transfer processes of ORR on graphene cluster with pentagon carbon ring at zigzag edge: (a) OOH adsorbed on carbon atom, (b) O-O bond breakage, and a water molecule formed, (c) OH molecule formed, and (d) two water molecules departing from graphene surface; The larger grey, red and smaller white balls denote to carbon, oxygen and hydrogen atoms, respectively.

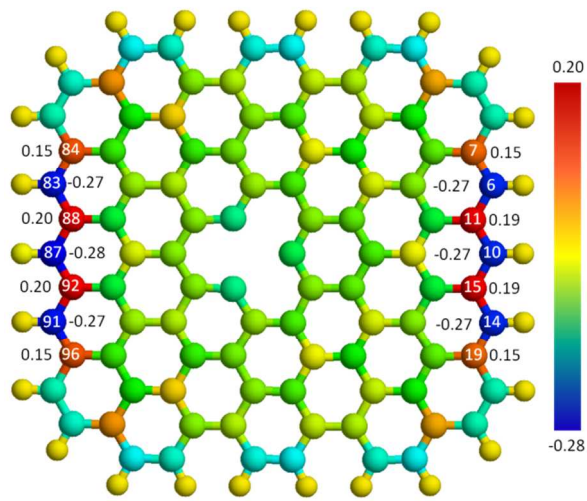
Figure 4. Two electron transfer processes of ORR on graphene cluster with pentagon-pentagon-octagon chains (GLD-558-01) (because of the size reason, just show part of structure): (a) OOH adsorbed on carbon atom #65, and (b) H₂O₂ molecule formed and departing from the graphene surface; The larger grey, red and smaller white balls denote to carbon, oxygen and hydrogen atoms, respectively.

Figure 5. Reaction free energy diagram for four-electron transfer oxygen reduction reaction over graphene clusters with a pentagon carbon ring at zigzag edge (a) and a GLD-558-01 grain boundary (b) based on the energy of table 1. The blue lines show the results at zero cell potential ($U=0$), the red lines stand for the results at potential $U= 0.57V$ (a), and $U= 0.91V$ (b), and the green lines indicate the energy at potential $U= 1.23 eV$.

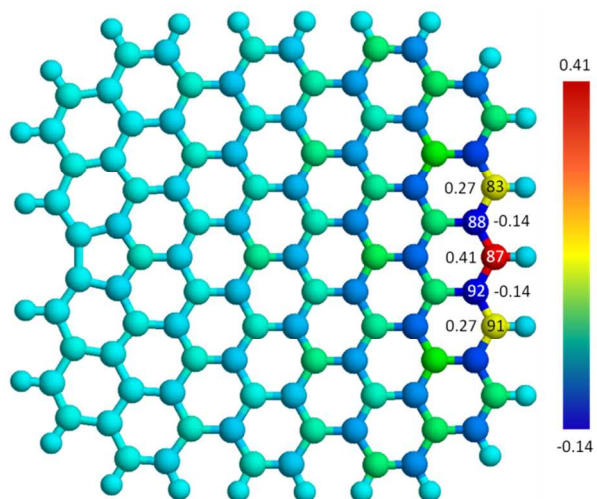
Figure 6. Reaction energy diagram of ORR on (a) PZ, and (b) GLD-558-01 defective graphene clusters



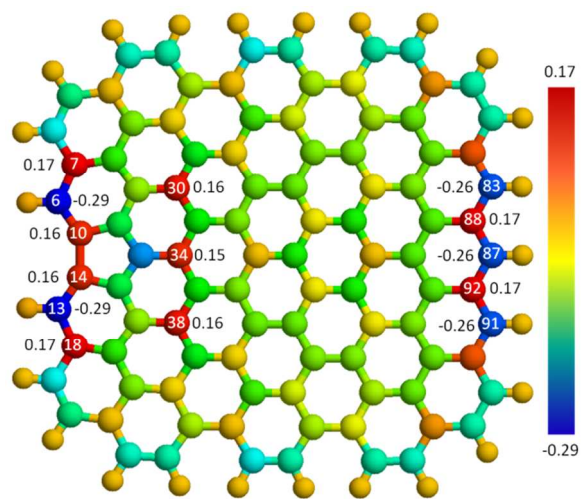
(a)



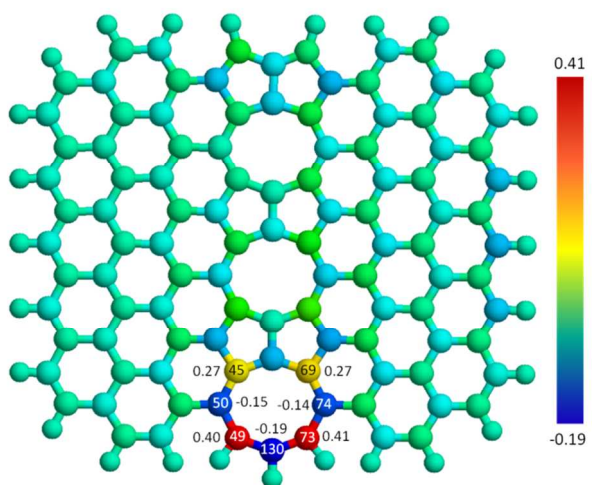
(b)



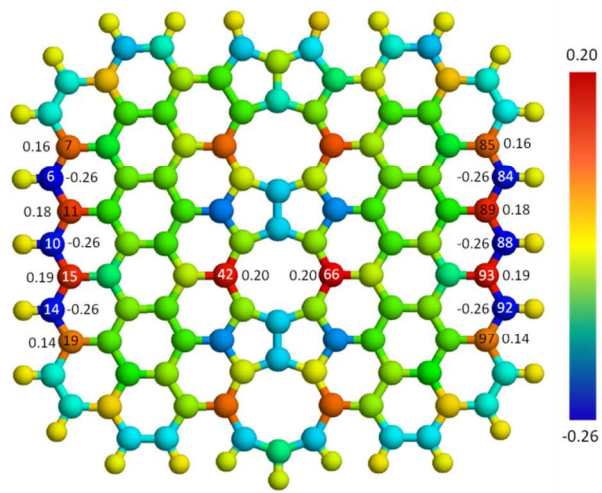
(c)



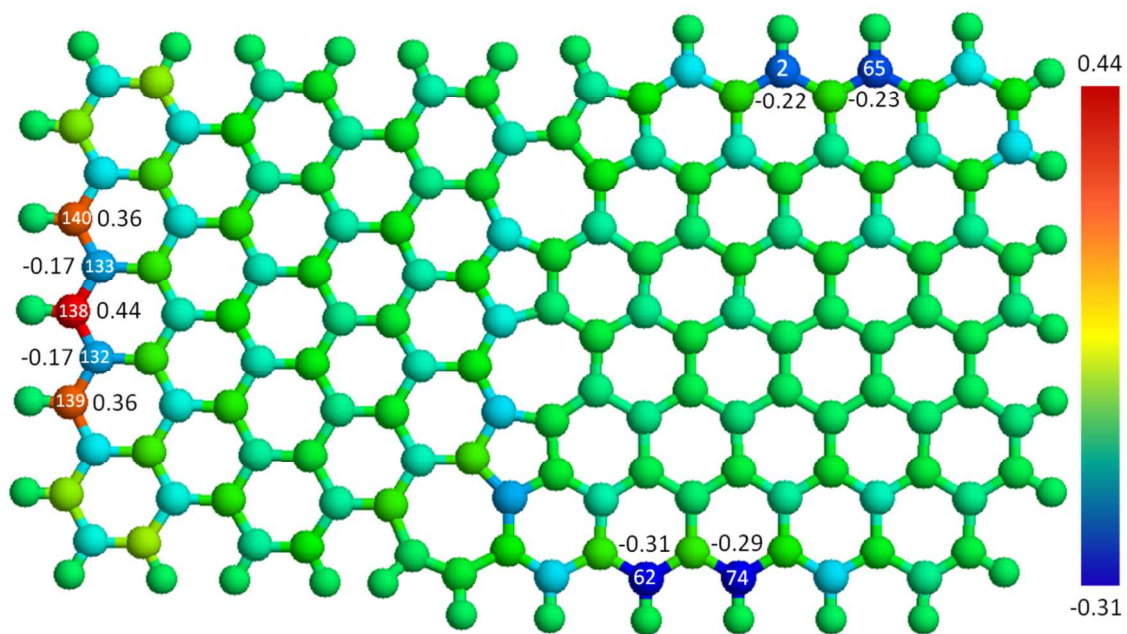
(d)



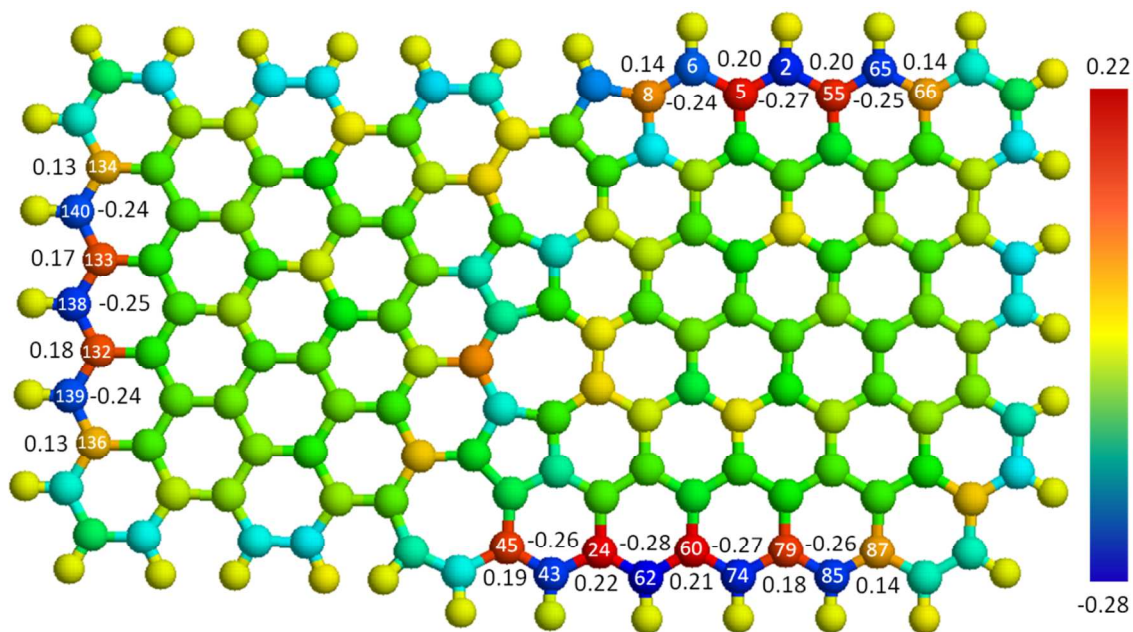
(e)



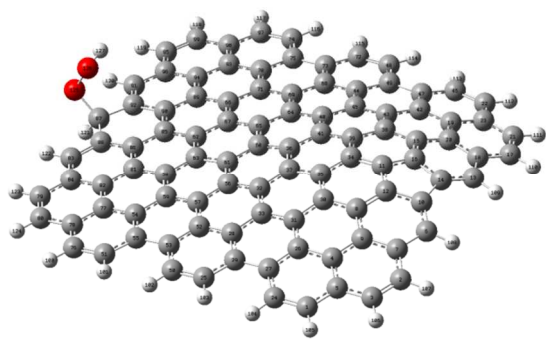
(f)



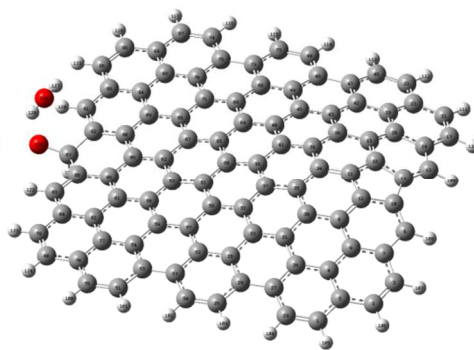
(g)



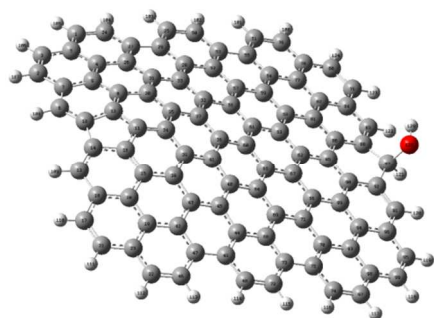
(h)



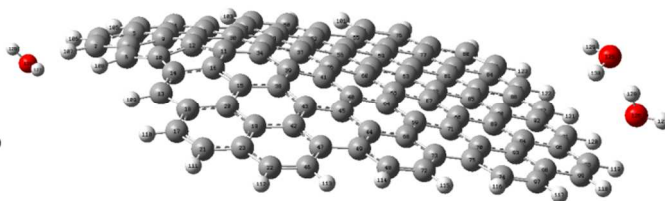
(a)



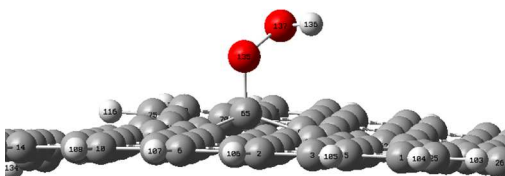
(b)



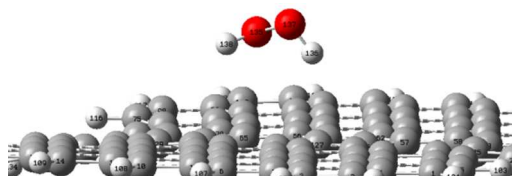
(c)



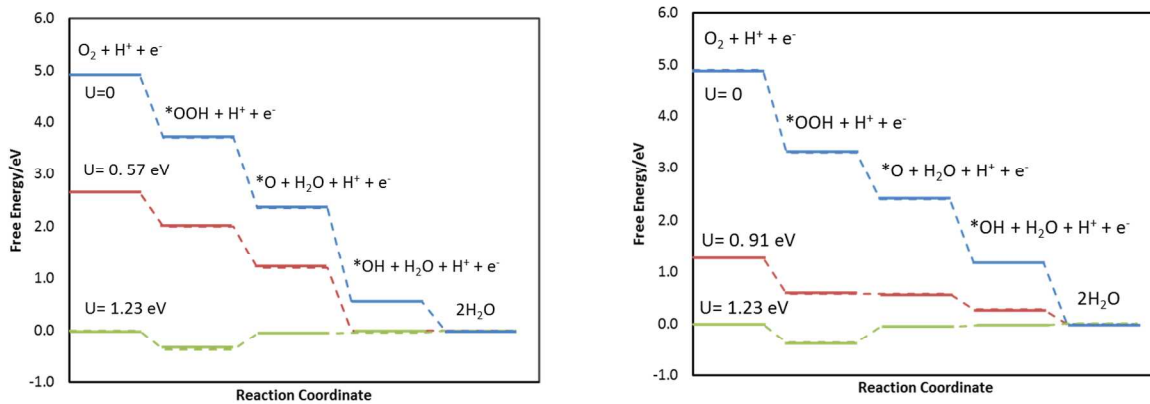
(d)



(a)

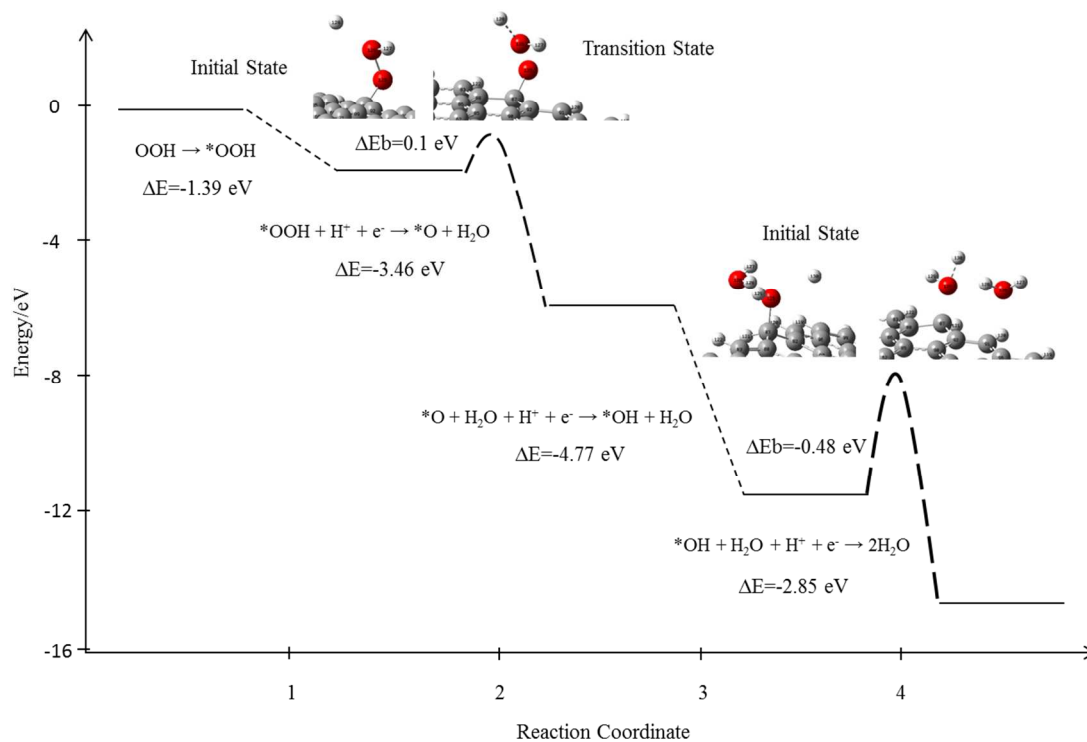


(b)

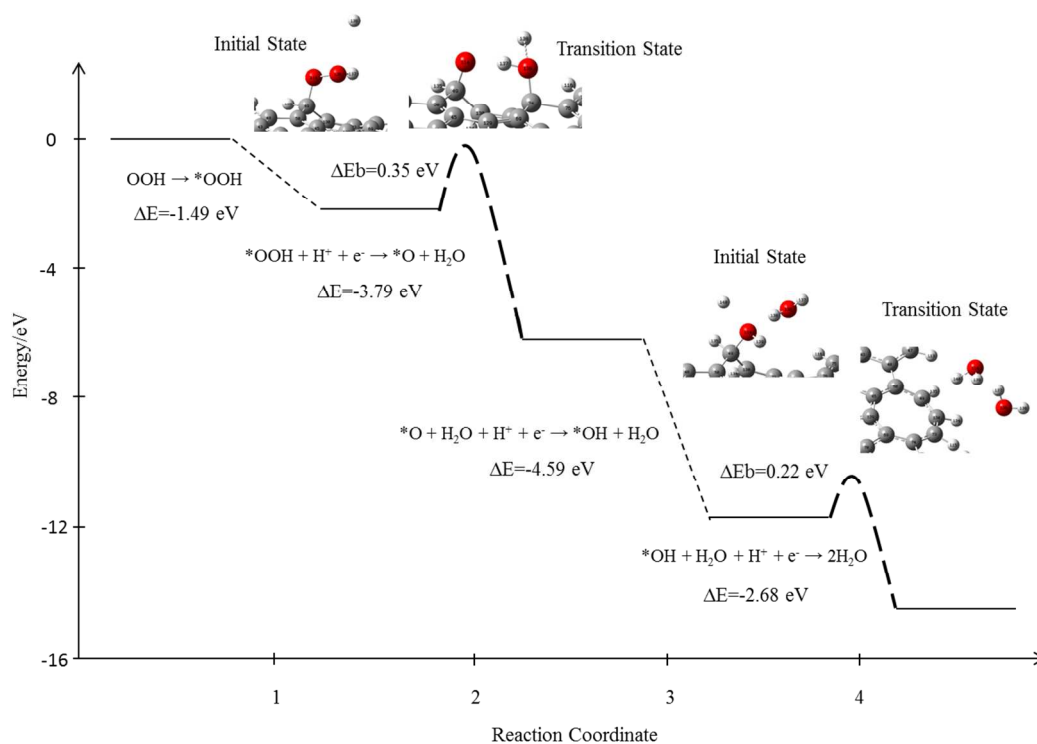


(a)

(b)



(a)



(b)

Table of Contents (TOC) Image

